Published in final edited form as:
Biochemistry. 2013 July 2; 52(26): 4439–4450. doi:10.1021/bi400283r.

Structural Basis of Multisite Single-Stranded DNA Recognition and *ACTA2* Repression by Purine-Rich Element Binding Protein B (Purβ)†

Amy E. Rumora[‡], **Shu-Xia Wang**[§], **Lauren A. Ferris**[‡], **Stephen J. Everse**[‡], and **Robert J. Kelm Jr.**[‡,§,∥,*]

[‡]Department of Biochemistry, University of Vermont College of Medicine, Burlington, VT 05405

[§]Department of Medicine, University of Vermont College of Medicine, Burlington, VT 05405

[∥]Department of Cardiovascular Research Institute, University of Vermont College of Medicine, Burlington, VT 05405

Abstract

A hallmark of dysfunctional fibroblast to myofibroblast differentiation associated with fibrotic disorders is persistent expression of *ACTA2*, the gene encoding the cyto-contractile protein smooth muscle α-actin. In this study, a *PURB*-specific gene knockdown approach was used in conjunction with biochemical analyses of protein subdomain structure and function to reveal the mechanism by which purine-rich element binding protein B (Purβ) restricts *ACTA2* expression in mouse embryo fibroblasts (MEFs). Consistent with the hypothesized role of Purβ as a suppressor of myofibroblast differentiation, stable short hairpin RNA-mediated knockdown of Purβ in cultured MEFs promoted changes in cell morphology, actin isoform expression, and cell migration indicative of conversion to a myofibroblast-like phenotype. Promoter-reporter assays in transfected Purβ knockdown MEFs confirmed that these changes were attributable, in part, to de-repression of *ACTA2* transcription. To map the domains in Purβ responsible for *ACTA2* repression, several recombinant truncation mutants were generated and analyzed based on hypothetical, computationally-derived models of the tertiary and quaternary structure of Purβ. Discrete subdomains mediating sequence- and strand-specific *cis*-element binding, protein-protein interaction, and inhibition of a composite *ACTA2* enhancer were identified using a combination of biochemical, biophysical, and cell-based assays. Our results indicate that the Purβ homodimer possesses three separate but unequal single-stranded DNA-binding modules formed by subdomain-specific inter- and intramolecular interactions. This structural arrangement suggests that the cooperative assembly of the dimeric Purβ repressor on the sense strand of the *ACTA2* enhancer is dictated by the association of each subdomain with distinct purine-rich binding sites within the enhancer.

The myofibroblast is a unique cell type that exhibits an ensemble of phenotypic properties typical of a collagenous matrix-producing fibroblast and a contractile smooth muscle cell

†This work was supported by NIH grant R01 HL054281 and AHA grant 09GRNT2170060 to R.J.K. A.E.R. and L.A.F. were supported by NIH training grant T32 HL007594 (Kenneth G. Mann, PI).

*To whom correspondence should be addressed: Robert J. Kelm, Jr., Department of Medicine, Cardiology/Vascular Biology Unit, University of Vermont College of Medicine, Colchester Research Facility, 208 South Park Drive, Colchester, VT 05446, Tel: (802) 656-0329; Fax: (802) 656-8969; robert.kelm@uvm.edu.

SUPPORTING INFORMATION AVAILABLE

Table S1, Figures S1 to S11, and an expanded methods section. This material is available free of charge via the Internet at http://pubs.acs.org.

(1). In the body, pre-formed myofibroblasts play an important structural role in certain developing and adult tissues and organs (1, 2). On the other hand, emergent myofibroblasts are critical to the formation and remodeling of granulation tissue during wound healing as they provide the contractile machinery and mechanical strength necessary for wound closure (3-5). While transient differentiation of resident connective tissue fibroblasts to myofibroblasts is a normal physiological response to tissue injury, persistent myofibroblast activation is associated with hypertrophic scarring, pathologic organ fibrosis, aberrant vascular remodeling, and dysfunctional stromal responses to neoplasia (6-9). Consequently, an improved understanding of the molecular mechanisms underlying myofibroblast *trans*-differentiation may reveal novel drug targets to limit scarring, fibrosis, and tumor progression.

Among the markers of myofibroblast conversion, expression of *ACTA2*, the gene encoding smooth muscle α-actin (SMαA)[3] is recognized as one of the key determinants of the transition to a contractile phenotype (10-12). Based largely on comparing *ACTA2* reporter gene activity in myogenic versus non-myogenic cell lines, early reports suggested that activation of *ACTA2* transcription in fibroblasts is mediated by serum-derived, growth factor-dependent signaling leading to induction of an otherwise repressed 5′ enhancer-promoter (13-15). Later studies revealed that the 5′ flanking region of *ACTA2* contains a variety of discrete but functionally-interacting *cis*-elements that serve as binding sites for certain muscle-associated, growth factor-inducible, or basal *trans*-activators found in *ACTA2*-expressing fibroblasts (16-19). In particular, combinatorial interactions between a transcription enhancer factor 1 (TEF1)-binding muscle CAT (MCAT) motif, two serum response factor (SRF)-interacting CArG boxes, and several specificity protein 1 and 3 (Sp1/3)-binding GC-rich elements are necessary to drive high level *ACTA2* transcription in differentiating myofibroblasts (17, 20). Conversely, in undifferentiated fibroblasts, the activity of a composite MCAT/CArG/GC box enhancer is apparently suppressed by several single-stranded DNA (ssDNA)-binding repressors that interact with the opposing strands of an asymmetric polypurine/polypyrimidine-rich (Pur/Pyr) tract containing the core MCAT motif (15, 21). Cell-based promoter mutagenesis studies in conjunction with nucleoprotein interaction analyses with double-stranded and single-stranded probes led to the identification of purine-rich element binding proteins A and B (Purα and Purβ) and Y-box binding protein 1 (YB-1) as the key factors in strand-specific Pur/Pyr tract recognition and repression of the composite *ACTA2* enhancer (17, 22).

Purα and Purβ are members of a small family of nucleic acid-binding proteins that interact with purine-rich ssDNA or RNA sequences homologous to the so-called PUR element originally described in eukaryotic gene flanking regions and origins of DNA replication (23-25). Despite the fact that Purα and Purβ share ~70% sequence identity and exhibit similar ssDNA-binding and helix-destabilizing properties *in vitro* (26-28), comparative gain-of-function and loss-of-function analyses conducted in transiently-transfected fibroblasts and vascular smooth muscle cells point to Purβ as the dominant repressor of *ACTA2* in these cell types (29, 30). In keeping with its general biological role as a potent repressor of genes that encode contractile proteins, Purβ has also been reported to negatively-regulate *MYH6* and *MYH7* in cardiac and skeletal myocytes (31-33). More recent studies suggest that Purβ repressor expression in muscle cells is tightly controlled at the post-transcriptional level by certain muscle-restricted microRNAs to ensure appropriate myofiber composition for sustained cardiac and skeletal muscle performance in response to stress (34, 35).

Apart from hydrodynamic analyses revealing that Purβ can reversibly self-associate to form an elongated homodimer in the absence of ssDNA (36), comparatively little is known about the higher order structural domains in either the Purβ monomer or dimer that confer specific and high-affinity interaction with purine-rich elements in *ACTA2* or any other target gene.

A previous report demonstrated that Purβ interacts in a sequential and cooperative manner with the sense strand of the MCAT-containing Pur/Pyr element from mouse *ACTA2* to form a high affinity 2:1 Purβ:ssDNA complex (37). While the primary structure of Purβ is similar to Purα in terms of the presence of three distinct regions of internal homology (dubbed PUR repeats I, II, and III) (38), Purβ contains several unique intervening sequences with high glycine and proline content that may affect the structural and functional properties of the protein (26). Importantly, the x-ray crystal structure of a truncated version of *Drosophila melanogaster (Dm)* Purα (amino acids 40-185) revealed a monomeric Whirly fold-like DNA-binding domain formed by the intramolecular interaction of the first two PUR repeat sequences (39). On the other hand, we recently identified a core tryptic fragment of Purβ (amino acids 29-305) that contains all three PUR repeats, self-associates in the absence of nucleic acid, and retains the ability to interact with the purine-rich strand of the *ACTA2*-derived MCAT element with high-affinity and specificity (40). In this study, the putative biological role of Purβ in suppressing *ACTA2* expression and restricting myofibroblast cyto-differentiation was first validated via a stable gene knockdown approach. *In silico* modeling of protein structure coupled with empirical analyses of protein function were then used to delineate the relevant domains in Purβ that mediate *ACTA2*-specific nucleoprotein interaction and repression of the composite MCAT/CArG/GC box enhancer.

MATERIALS AND METHODS

Cell culture and extraction

AKR-2B MEF cell lines stably-transduced with lentiviral vectors encoding a *PURB* transcript-specific short hairpin RNA (shRNA) or a scrambled control RNA were generated as described in (30). Subcloned cell lines were propagated in McCoys 5A medium (Gibco™/Invitrogen) containing 5% heat-inactivated fetal bovine serum (FBS) and 10 μg/ml blasticidin in a humidified 5% CO_2 incubator and studied at passage number 5 to 15. Phase contrast images of live cells were obtained on a Zeiss Axiovert model 200 inverted microscope equipped with an AxioCam MRm digital camera. Assays used to compare the growth and migratory properties of derived cell lines are detailed in Supporting Information. In timed growth factor-treatment experiments, cells were seeded at a fixed density and then switched to serum-free MCDB-402 medium (JRH Biosciences) for 36 to 48 h. Cells were then treated for 24 h with either 10% FBS or 2.5 ng/ml recombinant human transforming growth factor β1 (TGF-β1) (R & D Systems) diluted in MCDB-402 medium. Confluent monolayers of growth factor-stimulated cells were washed three times with ice-cold phosphate buffered saline (PBS) and then extracted with 1× Reporter Gene Assay Lysis Buffer (Roche Applied Science) supplemented with protease inhibitors 0.5 mM phenylmethanesulfonyl fluoride and 1 μg/ml each of pepstatin A, leupeptin, and aprotinin. Soluble lysates and cell remnants were collected by centrifugation at 15,800 × *g* for 10 min at 4°C. Total protein content in cleared lysates was measured by BCA™ Protein Assay (Thermo Scientific) using bovine serum albumin (BSA) as a standard. Insoluble pellets were further extracted with a denaturing solvent consisting of 8 M urea, 100 mM sodium phosphate, 10 mM Tris-Cl pH 8.0 plus protease inhibitors. Denatured lysates were cleared by centrifugation and assayed for protein content as described above.

Promoter:reporter constructs

Murine *ACTA2* promoter-chloramphenicol acetyltransferase reporter constructs (pVSMP8-CAT and pVSMP4-CAT) have been described elsewhere (14, 30, 41). The corresponding *ACTA2* promoter-luciferase reporters were constructed as follows. A ~3.6 kb fragment was released from pVSMP8-CAT by sequential treatment with *Sph*I, mung bean nuclease, and *Bam*HI. A ~240 bp insert was released from pVSMP4-CAT by sequential treatment with *Sal*I, mung bean nuclease, and *Bam*HI. Restriction fragments were ligated into *Sma*I/*Bgl*II-

digested and alkaline phosphatase-treated pGL3-Basic vector (Promega) to generate pVSMP8-Luc and pVSMP4-Luc. Following transformation into *E. coli* HB101 cells, ampicillin-resistant clones were selected for propagation and plasmid purification (Roche Applied Science). The fidelity of plasmid constructs was confirmed by restriction enzyme digestion followed by automated DNA sequencing performed by the Vermont Cancer Center DNA Analysis Facility.

Expression vectors

Bacterial and mammalian expression vectors encoding full-length, N-terminal hexahistidine-tagged mouse Purβ (pQE30-NHis-Purβ and pCI-NHis-Purβ) were described in previous reports (17, 22). Expression plasmids encoding NHis-Purβ truncation proteins corresponding to amino acids 41-112 (Purβ I), 125-210 (Purβ II), 209-303 (Purβ III), 41-210 (Purβ I-II), 125-303 (Purβ II-III), and 41-303 (Purβ I-II-III) were constructed following a similar strategy outlined in (29) and as further detailed in Supporting Information.

Monoclonal antibodies

With the exception of antibody screening assays, all other procedures involved in generating murine and rat monoclonal antibodies (mAbs) recognizing Purα and/or Purβ were carried out by a commercial vendor (Green Mountain Antibodies). These included rodent immunization, fusion of mouse or rat splenocytes with NS-1 myeloma cells, subcloning of hybridoma cells (2 rounds), and *in vitro* production, purification, and isotype/subclass determination of derived mAbs. The specific antigens used for immunization were keyhole limpet hemocyanin-coupled peptides corresponding to amino acid sequences B42-69, B302-324, and A291-313 of mouse Purβ and Purα, respectively (22). Animals were immunized with each individual peptide or a combination of all three peptides. The relative affinity and specificity of purified mAbs were evaluated by direct enzyme-linked immunosorbent assay (ELISA) using immobilized peptides or full-length NHis-Purα or NHis-Purβ as described in Supporting Information and shown in Figure S1.

Computational modeling of protein structure

A homology model of *Mus musculus* (*Mm*) Purβ was generated based on the structure of *Drosophila melanogaster* (*Dm*) Purα repeats I-II (amino acids 40-185) using web-based modeling servers and a bioinformatics approach described previously (38, 39). A pair-wise multiple sequence alignment of *Mm* Purβ and *Dm* Purα indicating 52% sequence identity was obtained using ClustalW (42, 43). The sequence alignment was submitted to the HHrepID and PSIPRED web servers (44, 45) under default parameters to identify repeated sequences and predict secondary structural elements within Purβ (26). To generate a model consistent with these results, the FASTA sequence of *Mm* Purβ was submitted to the I-TASSER web server (46, 47) to generate a homology model of Purβ repeats I-II using *Dm* Purα I-II (3K44) as a template (39). On the basis of the internal sequence homology of the three Purβ repeats, Purβ III was independently predicted by SWISS-MODEL (48-50) by threading the sequence of the third Purβ repeat onto the structure of *Dm* Purα I-II. Predicted intermolecular interaction between two Purβ III repeats was modeled by rotating the *Mm* Purβ III repeats of two monomers into an extended conformation and aligning them on *Dm* Purα I-II using Coot (51). Energy minimization of the Purβ homodimeric homology model was completed using CNS version 1.2 (52, 53) to relax close contacts and to regularize local bond and angle geometry. Computationally-derived structures were viewed and depicted using PyMOL (54).

Recombinant protein purification

Full-length NHis-Purβ and selected truncation proteins were expressed in and isolated from *E. coli* JM109 cells using chromatographic methods optimized for each particular recombinant protein as detailed in Supporting Information. NHis-Purβ-enriched fractions obtained by metal chelate affinity, heparin affinity, or size exclusion chromatography (SEC) were monitored for purity by sodium dodecyl sulfate-polyacrylamide gel electrophoresis (SDS-PAGE) under reducing conditions and staining with Coomassie® Brilliant Blue R-250. Wide range SigmaMarker™ proteins (Sigma-Aldrich) were used as molecular weight standards. The protein concentration of pooled fractions was determined by absorbance measurement using theoretical molar extinction coefficients at 280 nm of 20,400 M^{-1} cm^{-1} for full-length NHis-Purβ and NHis-Purβ I-II-III, 7,450 M^{-1} cm^{-1} for NHis-Purβ I-II, and 12,950 M^{-1} cm^{-1} for NHis-Purβ III (55). Protein preparations were routinely screened to ensure the absence of contaminating nucleic acid as previously described (36). Protein preparations were also monitored for the presence of nuclease activity by incubating 1.0 μM protein stocks with 2 μg of either pBLCAT3 plasmid or M13mp18 ssDNA (Bayou Biolabs) for 1 h at 37°C. The integrity of the DNA substrates was then evaluated by agarose gel electrophoresis. Absence of contaminating nuclease activity in recombinant Purβ preparations was established based on comparison to DNA substrates treated in parallel with 10^{-1} to 10^{-5} units of DNase I (Invitrogen).

Calibrated SEC and circular dichroism (CD) spectroscopy

The quaternary state of purified truncation proteins was determined by SEC on a 1.5 × 100 cm Sephacryl® 200 HR column calibrated with molecular weight standards blue dextran, BSA, ovalbumin, carbonic anhydrase, cytochrome C, and DNP aspartate (36). The foldedness of recombinant proteins was assessed by CD spectroscopy. All proteins were analyzed on a Jasco model 815 spectrometer after dialysis into buffer consisting of 50 mM Tris-Cl pH 7.5, 300 mM NaCl, 0.5 mM EDTA, and 0.5 mM tris(2-carboxyethyl)phosphine hydrochloride (TCEP). Multiple wavelength scans were recorded at 1 nm intervals from 195 to 280 nm on 5.0 μM protein solutions in a 1 mm cuvette at 25°C. Raw CD data were analyzed as previously described (40).

Single-stranded DNA-binding assays

Direct or competitive colorimetric microplate-based assays were conducted with purified proteins and a 3′ biotinylated ssDNA probe corresponding to the purine-rich strand of the murine *ACTA2* 5′-flanking sequence from −195 to −164 (PE32-bF) as previously described (40, 56). In the direct ssDNA-binding format, solid-phase Purβ-PE32-bF complexes were detected by ELISA using primary rabbit antibodies directed against amino acids 210-229 or 302-324 of mouse Purβ (22) or the NHis tag (His probe H-15 from Santa Cruz Biotechnology, Inc. or anti-6-His from Bethyl Laboratories, Inc.). In the competitive binding format, solid-phase nucleoprotein complexes were detected with ExtrAvidin®-peroxidase (Sigma-Aldrich). Log [protein] vs. absorbance datasets were fit to four parameter variable slope equations to determine EC50 or IC50 values depending on the format of the assay (Prism 5, Version 5.04, Graphpad Software, Inc.).

Protein-protein interaction assay

Protein-protein interaction was assessed in an ELISA format using microtiter wells (Costar® EIA/RIA 96 well plate, certified high binding, Corning Inc.) coated with 200 nM NHis-Purβ or selected truncation proteins as previously described (30, 56). Nuclear extracts prepared from exponentially growing AKR-2B MEFs served as a source of protein binding partners of Purβ (57). The primary antibodies used for detection of solid-phase protein-protein complexes included rabbit anti-mouse Puraα 291-313 (22), rabbit anti-mouse YB-1 (MSY1)

242-269 (22), and rabbit anti-mouse TEF1 1-15 (17). Commercial rabbit polyclonal antibodies against SRF (G-20), Sp1 (H-225 and PEP-2), and Sp3 (D-20) were from Santa Cruz Biotechnology, Inc.

Transient transfection assay

AKR-2B MEFs were seeded into 6 well plates at 4.0×10^4 cells per well in McCoys 5A medium with 5% FBS. Primary mouse aortic outgrowth smooth muscle cells (AoSMCs) (30) were seeded at 2.5×10^4 cells per well in DMEM with 10% FBS. After an overnight incubation at 37°C in a 5% (MEFs) or 10% (AoSMCs) CO_2 incubator, adherent cells were transfected with 2 μg of total DNA using jetPEI™ reagent (PolyPlus-transfection) at a ratio of 1.5 μl per μg of DNA. Transfection solutions typically contained 0.9 μg of pVSMP8- or pVSMP4-CAT or luciferase reporters, 0.1 μg of pSV40-β-Gal control reporter, and 1.0 μg of expression plasmid. After 48 h incubation at 37°C, cells were washed with PBS and then extracted with 1× Passive Lysis Buffer (Promega) supplemented with protease inhibitors. Total protein content was determined by BCA™ or Bradford assay and individual reporters were measured with the use of a CAT or β-Gal ELISA kit (Roche Applied Science), Luciferase Assay System (Promega), or *ortho*-nitrophenyl-β-galactoside chromogenic substrate assay. Numerical datasets were subjected to one-way analysis of variance and Tukey's multiple comparison test with significance set at $p < 0.05$ (Prism 5, Version 5.04, Graphpad Software, Inc.). In some instances, transfected cells were processed by sequential extraction using a subcellular protein fractionation kit as directed by the manufacturer (Thermo Scientific).

Immunoblotting

Samples were prepared for SDS-PAGE by dilution of concentrated cell lysates into 6× sample preparation buffer (120 mM Tris-Cl pH 6.8, 3% w/v SDS, 30% v/v glycerol, 0.03% w/v bromophenol blue). For less concentrated cell lysates, soluble protein was precipitated by adding 5 volumes of ice-cold ethanol to 1 volume of cell lysate and incubating for at least 1 h at −20°C. Precipitated protein was collected by centrifugation and dissolved in 1× SDS-PAGE loading buffer. Samples were supplemented with 5% v/v 2-mercaptoethanol, heated for 3-5 min at 100°C, and subjected to slab gel electrophoresis on 10%, 12% or 15% w/v acrylamide:bisacrylamide (29:1) mini-gels or 4-20% precast gradient gels (Lonza). Molecular weight standards were run in parallel on each gel (BenchMark™ Prestained Protein Ladder, Invitrogen). Proteins were then electrotransferred to Immobilon®-P or Immobilon®-PSQ polyvinylidene difluoride membrane (Millipore) in 25 mM Trizma base, 192 mM glycine, 20% v/v methanol at 125 V for 90 min at 4°C. Transblots were probed with selected antibodies as described in (22). Primary and secondary antibodies used are listed in Supporting Information.

RESULTS

Derivation of Purβ knockdown MEFs

To assess the phenotypic consequence of Purβ loss-of-function in a multipotent mesenchymal cell type, a lentiviral shRNA expression system was used to stably-transduce AKR-2B MEFs owing to their high steady-state levels of Purα and Purβ and sensitivity to inducers of myofibroblast differentiation (20, 22, 58). As shown in Figure 1A, specific knockdown of Purβ (faster migrating band of doublet) was confirmed in two independently-derived blasticidin-resistant cell lines by Western blotting with the use of a newly-developed rat monoclonal antibody directed against a conserved PUR repeat I sequence present in both Purα and Purβ (specifically, amino acids 42-69 of Purβ). Importantly, Purα expression (slower migrating band of doublet) was not altered in either Purβ-only knockdown cell line (βI-B4 and β1-G7) compared to control cells transduced with scrambled RNA (βS-E6). For

the purpose of comparison, extract from a serendipitously-derived cell line deficient in Purα expression (βI-F3) was included on the gel to highlight differences in the electrophoretic mobility of bands corresponding to Purα and Purβ. To quantify relative differences in Purβ expression, a functional ELISA was used to measure Purβ ssDNA-binding activity in soluble extracts of each cell line (Figure 1B). In keeping with the results of Western blotting, Purβ ssDNA-binding activity was reduced by 2.5-2.7 fold in the βI-B4 and βI-G7 cells in comparison to the βS-E6 control cell line. Consistent with a dominant Purα loss-of-function phenotype (59), the Purα-deficient βI-F3 cell line exhibited a markedly enhanced rate of cell growth relative to Purβ-only knockdown and scrambled control cell lines and was thus excluded from detailed study (Figure S2).

Phenotypic properties of Purβ knockdown MEFs

Analysis of growing MEF cell lines by light microscopy revealed that Purβ-only knockdown cells adopt a more elongated spindle-like morphology in comparison to control cells expressing scrambled RNA (Figure 1C). A similar but less dramatic change in morphology is evident in cells co-deficient in Purα. These morphological differences were readily apparent in confluent cell monolayers as well (Figure S3). To investigate the physical basis for these changes in cell shape, the expression of cytoskeletal actin proteins was assessed by immunoblotting of detergent-soluble and detergent-insoluble lysates prepared from serum- or TGF-β1-stimulated MEF cell lines. In serum-stimulated cells, the soluble G-form of SMαA was the predominant actin isoform exhibiting enhanced expression in concert with Purβ knockdown although a slight increase in β-actin expression was detected as well (Figure 2A). Consistent with sensitization to TGF-β1-driven myofibroblast cyto-differentiation, a corresponding increase in both G- and F-form SMαA, but not β-actin, was seen in Purβ knockdown MEFs relative to the control cell line treated with TGF-β1 (Figure 2B). Purβ deficiency, however, did not promote acquisition of a smooth muscle cell-like protein expression pattern as other markers of smooth muscle differentiation including smooth muscle myosin and SM22α/transgelin were not detected by immunoblotting of either control or Purβ knockdown MEFs (data not shown). To determine whether increased expression of SMαA protein correlated with de-repression of *ACTA2* transcription, transient transfection assays were conducted using a minimal MCAT- and CArG-dependent *ACTA2* enhancer-promoter construct. As shown in Figure 2C, *ACTA2*-driven reporter expression was significantly increased in both Purβ knockdown cell lines in comparison to control cells implying that loss of Purβ repressor function is necessary and sufficient to promote *ACTA2* expression and myofibroblast differentiation in MEFs. In keeping with the known motility-restrictive properties of SMαA-containing myofilaments in cultured fibroblasts (60), Purβ knockdown MEFs also demonstrated a modest reduction in chemotactic migration toward serum growth factors as measured by Boyden chamber assay (Figure S4).

Homology modeling of Purβ tertiary and quaternary structure

To explore the physical basis for Purβ-mediated repression of *ACTA2* transcription, we first set out to computationally model the higher order structure of Purβ based on 1) sequence homology with other members of the purine-rich element binding protein family, and 2) the known x-ray crystal structure of *Dm* Purα 40-185. Primary sequence analysis of *Mm* Purβ using selected homology detection and structure prediction algorithms indicated that Purβ possesses the same linear arrangement of PUR repeat modules (designated I, II, III) as originally described in Purα (38, 39) (Figure 3A). The sequences encoding *Mm* Purα and *Mm* Purβ were threaded on the x-ray crystal structure of *Dm* Purα residues 40-185 (3K44) using SWISS-MODEL to assess the overall homology of the intramolecular PUR domain formed by PUR repeats I and II of each protein. As expected, the major differences were restricted to putative loop regions connecting the individual PUR I and II repeats while the

β-strand and α-helix forming sequences were virtually superimposable (Figure S5). To create a hypothetical structure of the full-length Purβ monomer, PUR repeat III was independently modeled using SWISS-MODEL and the tertiary structure of the entire protein was constructed on the basis of an I-TASSER generated template (Figure 3B). Like PUR repeats I and II, PUR repeat III is predicted to possess similar ββββα topology. However, a putative random coil-forming region located between PUR repeats II and III may impart some degree of flexibility as to the position of PUR repeat III relative to the intramolecular domain formed by PUR repeats I and II (Figure 3C). Consequently, dimerization may occur via formation of an intermolecular PUR domain composed of two self-associating PUR III repeats from two Purβ monomers (Figure 3D).

Structural analysis of computationally-derived Purβ subdomains

To test the models in Figure 3, a series of cDNAs were engineered to encode NHis-tagged Purβ truncation proteins corresponding to individual PUR repeat modules (Purβ I, Purβ II, Purβ III) or selected combinations thereof (Purβ I-II, Purβ II-III, Purβ I-II-III). The utility of recombinant NHis-Purβ as a reliable experimental surrogate for the native protein expressed in mammalian cells has been documented in previous studies (29, 37, 56). Sequence validated bacterial expression plasmids were transformed into *E. coli* cells and recombinant truncation proteins were produced for trial purification under both native and denaturing conditions. While metal chelate affinity enrichment of each Purβ truncation protein was possible under harsh denaturing conditions (data not shown), only Purβ I-II-III (residues 41-303), Purβ I-II (residues 41-210), and Purβ III (residues 209-303) were amenable to purification in non-denaturing solvents (Figure S6) and were found to exhibit CD spectra consistent with well-folded polypeptides (Figure S7). Hence, it appeared that Purβ I (residues 41-112), Purβ II (residues 125-210), and Purβ II-III (residues 125-303) were intrinsically unstable and/or mis-folded when expressed in *E. coli*. This observation is consistent with the putative requirement for intramolecular association of PUR repeats I and II or intermolecular association of two PUR III repeats to form a stably-folded subdomain (Figure 3). To confirm the predicted quaternary state of each isolated truncation protein, calibrated SEC was performed using loading concentrations well in excess of the reported K_d for the full-length Purβ dimer (36). As shown in Figure 4A and B, Purβ I-II-III eluted as a ~64 kDa dimer while Purβ I-II resolved as a ~18 kDa monomer. In agreement with its predicted role in mediating self-association, Purβ III eluted as a ~17 kDa dimer (Figure 4C).

ACTA2 repressor activity of Purβ subdomains

To assess the functional role of each putative Purβ subdomain in *ACTA2* repression, transient co-transfection assays were performed in MEFs and primary mouse AoSMCs using a full-length *ACTA2* construct (−1070 to +2582, VSMP8-Luc) as well as a minimal MCAT/CArG/GC box-dependent enhancer (−146 to +46, VSMP4-Luc) as specific transcriptional targets of Purβ (30). As shown in Figure 5B, full-length Purβ and the core I-II-III construct demonstrated comparable repressor activity toward both *ACTA2* reporters in MEFs. Importantly, Purβ I-II was the only other truncation protein to exhibit statistically significant repressor activity. Purβ III alone showed no inhibitory activity while Purβ II-III was only weakly repressive. In agreement with *E. coli* expression and purification studies, immunoblotting of non-denatured MEF lysates indicated stable expression of full-length Purβ, Purβ I-II-III, Purβ I-II, and Purβ III (Figure 5C). However, Purβ I, Purβ II, and Purβ II-III were either not readily detected or only seen after extracting detergent-insoluble cell remnants with a denaturing solvent (Figure 5D), again pointing to the intrinsic instability and/or mis-folding of these truncation mutants. Essentially identical results were obtained in co-transfection studies conducted with primary AoSMCs (Figure S8) supporting the conclusion that the relative *ACTA2* repressor activity of the stably-expressed truncation proteins is Purβ I-II-III > Purβ I-II ≫ Purβ II-III or Purβ III. Titration studies conducted in

AKR-2B MEFs using a fixed amount of VSMP8 reporter and varying amounts of expression plasmid confirmed that Purβ I-II-III and Purβ I-II are quantitatively distinct in terms of their *ACTA2* repressor activity (Figure 6).

Cis-element binding properties of Purβ subdomains

To assess whether the relative *ACTA2* repressor activity of each Purβ truncation protein correlated with differences in the affinity and/or specificity for target sites in the *ACTA2* promoter, colorimetric microplate-based assays were used to compare the ssDNA-binding properties of Purβ I-II-III, Purβ I-II, and Purβ III to full-length Purβ. The purine-rich sense strand of the 5′ *ACTA2* Pur/Pyr element containing a consensus core MCAT motif (italics) (GGGAGCAGAACAG*AGGAATG*CAGTGGAAGAGA, PE32-F) was chosen as a probe because it has multiple interacting binding sites (underlined) that permit formation of a high-affinity (macroscopic K_d ~ 0.3 nM) 2:1 Purβ:ssDNA complex (37). Initially, a titration experiment was performed to identify a minimal concentration of 3′ biotinylated PE32-F probe necessary to detect the interaction of each Purβ truncation protein by ELISA. Surprisingly, stable formation of Purβ I-II nucleoprotein complexes required a markedly higher concentration of ssDNA implying a significant difference in binding affinity of the monomeric subdomain relative to full-length Purβ, Purβ I-II-III, and Purβ III (Figure S9A). Titration assays conducted with a limiting concentration of PE32-bF (0.5 nM) highlighted the striking differences in the apparent ssDNA-binding affinity of the individual subdomains, Purβ III (EC50 = 1.80 ± 0.74 nM, n = 4) and Purβ I-II (EC50> 100 nM), relative to the full-length protein (EC50 = 0.16 ± 0.05 nM, n = 4) and Purβ I-II-III (EC50 = 0.22 ± 0.05 nM, n = 4) (Figure 7A and B). Consistent with a functional distinction between the separated dimerization and intramolecular subdomains, competition assays revealed that Purβ III (IC50 = 46 ± 15 nM, n = 3) and Purβ I-II (IC50 > 1000 nM) were much less effective than the composite Purβ I-II-III construct (IC50 = 1.0 ± 0.3 nM, n = 5) or the full-length protein (IC50 = 1.2 ± 0.2 nM, n = 5) at inhibiting the interaction of 0.5 nM PE32-bF with immobilized Purβ (Figure 7C). Despite these substantial differences in apparent ssDNA-binding affinity, the isolated Purβ III and Purβ I-II subdomains retained similar binding site specificity as demonstrated by their reduced interaction with mutant versions of PE32-bF containing heptathymidylate substitutions (T7) in place of 5′ or 3′ PUR and/or internal MCAT motifs (Figure 7D and Figure S9B).

Trans-acting factor binding properties of Purβ subdomains

To ascertain whether the isolated subdomains exhibited similar protein binding properties as full-length Purβ, an ELISA-based profiling assay was conducted using nuclear extract from AKR-2B MEFs as a natural source of potential Purβ interaction partners. Recombinant Purβ proteins were immobilized on microtiter wells at a saturating coating concentration (200 nM) and then assayed for their ability to capture specific transcription factors implicated in *ACTA2* activation or repression. Consistent with previous findings (30, 56), full-length Purβ demonstrated preferential interaction with its co-repressor partner MSY1 relative to other factors screened using this assay format (Figure 8). Interestingly, Purβ I-II-III exhibited an even greater binding capacity for MSY1, while the isolated Purβ I-II and Purβ III subdomains displayed markedly reduced interaction with MSY1. In contrast, Purβ I-II showed a clear preference for interaction with the *ACTA2 trans*-activator Sp3, while Purβ III exhibited little or no Sp3 binding activity. Essentially identical results were obtained using nuclear extract diluted in binding buffer supplemented with reducing agent (Figure S10). This was done to ensure that the differences observed in the binding properties of individual Purβ truncation proteins were not attributable to anomalous protein oxidation.

DISCUSSION

The transient differentiation of stromal fibroblasts to contractile, SMαA-expressing myofibroblasts is an essential and tightly-regulated component of the wound healing process. Conversely, sustained stromal myofibroblast activation is pathologic as it often promotes aberrant tissue remodeling (61). Because SMαA expression is a biochemical hallmark of the myofibroblast phenotype, a better understanding of the regulatory factors that mediate *ACTA2* transcription and translation in fibroblasts may reveal novel targets for therapeutic intervention to limit destructive fibrocontractile remodeling associated with scarring, fibrosis, and tumor progression. Among the factors implicated in *ACTA2* regulation in fibroblasts, Purα and Purβ are unique in that they apparently repress gene transcription by forming nucleoprotein complexes with purine-rich ssDNA in such a way as to block *trans*-activator recognition of cognate double-stranded binding sites within the composite MCAT/CArG/GC box enhancer (16, 17, 30, 62).

In view of a growing body of evidence suggesting that Purβ may play a central role in repressing genes encoding muscle-restricted isoforms of actin and myosin in both myogenic and non-myogenic cell types (31-35), we initially sought to confirm that deficiency of Purβ in MEFs would necessarily promote the acquisition of a myofibroblast phenotype *in vitro*. To do so, we transduced MEFs using a lentivirus-based shRNA transgene delivery system to knockdown the expression of Purβ in a specific, stable, and constitutive manner. Analyses of two independently-derived cell lines showed that a relatively modest decrease in Purβ expression (~60-70% knockdown) was sufficient to switch cells to a myofibroblast-like phenotype as exemplified by characteristic changes in cell morphology, SMαA expression, TGF-β1 inducibility, and chemotactic migration (Figures 1, 2, S3 and S4). Importantly, these changes occurred in the absence of any substantive effect on cell growth suggesting that Purβ does not participate in the direct regulation of cell cycling as has been reported for Purα (63-68).

To better understand the structural basis for Purβ-mediated repression of *ACTA2*, we employed web-based homology modeling servers to generate computational models of the Purβ monomer and dimer based on the known x-ray crystal structure of *Dm* Purα residues 40-185 (39). As previously described for Purα (38), the HHrepID web server identified three regions of internal sequence homology termed PUR repeats I, II, and III (Figure 3). Homology modeling suggested that each PUR repeat is similarly structured with respect to the arrangement of four β-stands and one α-helix. By analogy to the tertiary structure of *Dm* Purα I-II, *Mm* Purβ I-II is predicted to fold in such a way as to form an intramolecular PUR domain with features resembling a Whirly class-like DNA-binding fold (39). Although the PUR III repeat of Purβ is also predicted to adopt ββββα topology, the α-helical region is substantially longer than in PUR repeats I and II owing to the presence of the so-called “psycho” motif spanning residues 264-291 (26). This sequence is predicted to form an extended amphipathic α-helix, which may facilitate protein-protein interaction. In one hypothetical model of the Purβ monomer, the PUR III repeat is depicted as packing against the PUR I-II intramolecular domain (Figure 3B). However, previous hydrodynamic studies showed that full-length Purβ reversibly self-associates to form an elongated homodimer (36). Therefore, we speculated that the glycine-rich sequence spanning residues 210-229 may impart some degree of internal flexibility allowing the PUR III repeat region to extend away from I-II (Figure 3C). The interaction of two PUR III repeats to form an intermolecular PUR domain would necessarily give rise to an elongated Purβ homodimer composed of three distinct modules (Figure 3D).

Based on these deduced homology models, we created a set of expression vectors encoding His-tagged Purβ truncation proteins containing single or selected combinations of PUR

repeats I, II, and III. Trial purifications from *E. coli* indicated that stable expression and folding of Purβ requires the formation of intra- and/or intermolecular subdomains. For example, Purβ I, Purβ II, and Purβ II-III constructs were poorly expressed and/or only detectable in denatured lysates. Conversely, full-length Purβ, Purβ I-II-III, Purβ I-II, and Purβ III were each highly expressed and readily purified under non-denaturing conditions. Moreover, their respective CD spectra were indicative of well-folded polypeptides. The results of calibrated SEC analysis confirmed the predicted quaternary state of each purified truncation protein and indicated that PUR repeat III constitutes the dimerization domain of Purβ (Figure 4). These findings are entirely consistent with the reported quaternary structures of *Dm* Purα I-II and *Dm* Purα I-II-III (39). Although the Purα homodimer has been proposed to adopt a Z-like shape based on results of small angle-X-ray scattering (39), the exact orientation and relation of the intra- and intermolecular subdomains in the Purβ homodimer is currently unknown.

To evaluate the capacity of each Purβ truncation protein to repress *ACTA2* transcription, we performed *ACTA2*-luciferase reporter gene assays in both MEFs and AoSMCs. As expected, the relative expression/stability of each Purβ construct in mammalian cells was similar to that seen in *E. coli*. Of the truncation proteins expressed, only the dimerization-competent Purβ I-II-III core construct and the Purβ I-II intramolecular subdomain were consistently found to repress both the complete and minimal *ACTA2* enhancer-promoter in both cell types (Figures 5 and S8). However, while Purβ I-II-III repressed the promoter to the same extent as the full-length protein, Purβ I-II exhibited ~50% less repressor activity. The intrinsically weaker activity of Purβ I-II was validated by titration experiments conducted over an extended range of expression vector concentrations pointing to the necessity of the PUR III repeat for full repressor function (Figure 6). Interestingly, forced expression of the Purβ III dimerization domain by itself did not affect the *ACTA2* enhancer-promoter owing, in part, to the apparent inability of this construct to enter the nucleus when separated from Purβ I-II intramolecular domain (Figure S11). However, in the context of the full-length protein and the Purβ I-II-III core construct, we surmise that the PUR repeat III likely promotes more efficient *ACTA2* repression by mediating the formation of a dimeric repressor capable of multisite ssDNA-binding within the confines of the nucleus.

Previous high resolution structural analyses of the 5′-flanking region of *ACTA2* during myofibroblast differentiation revealed that an asymmetric Pur/Pyr tract spanning nucleotides −210 to −150 is hypersensitive to modification by chemical probes that preferentially react with unpaired nucleobases (58). This region contains a consensus MCAT motif and a TGF-β1 response element that appear to function in conjunction with downstream CArG and GC boxes to mediate high level *ACTA2* transcription in fibroblasts (16, 17, 20). Consequently, we have chosen to focus our efforts on characterizing the interaction of Purβ with the MCAT region of the *ACTA2* enhancer-promoter due to its high Pur/Pyr asymmetry and apparent propensity to transiently adopt non B-form structures *in vivo* (58). In this regard, a prior study from our lab reported that Purβ interacts with the 32 nt purine-rich strand of the *ACTA2* MCAT element (dubbed PE32-F, −195 to −164) via a cooperative binding mechanism to generate a high-affinity 2:1 Purβ:ssDNA complex (37).

To test the importance of protein dimerization in facilitating the interaction of Purβ with PE32-F, the relative ssDNA-binding affinity and specificity of full-length Purβ and the core I-II-III protein were compared to the isolated intra- and intermolecular subdomains using both direct and competitive ssDNA-binding assays. Because these microplate-based colorimetric assays were performed under intrinsically non-equilibrium conditions, it was not possible to determine precise quantitative differences between Purβ I-II-III and the full-length protein. Despite this technical limitation, the Purβ I-II-III core construct did appear to bind PE32-F with comparable affinity and specificity to full-length Purβ under the assay

conditions employed (Figure 7). Moreover, the biochemical properties of Purβ I-II-III (residues 41-303) defined in this study are analogous to those of a His tag-free core tryptic fragment of Purβ (residues 29-305) described in an earlier report (40). Interestingly, while the Purβ I-II and Purβ III subdomains each displayed a lower apparent affinity for PE32-F than Purβ I-II-III, the intermolecular subdomain bound more tightly to ssDNA than the intramolecular subdomain. The functional non-identity of the isolated Purβ I-II and Purβ III subdomains suggests that the native Purβ homodimer contains three separate but unequal ssDNA-binding modules. This structural arrangement reinforces the concept that stable nucleoprotein complex assembly on the *ACTA2* MCAT element likely involves the recognition of multiple binding sites by Purβ (37). In support of this assertion, mutation of all three PUR elements in PE32-F was necessary to completely eliminate ssDNA-binding by full-length Purβ, the I-II-III core, and each subdomain (Figure 7D).

Another defining attribute of Purβ structure and function uncovered in this report is that the individual subdomains of Purβ differ in their capacity to interact with certain transcription factors relevant to *ACTA2* regulation in fibroblasts. In particular, the Purβ I-II intramolecular subdomain was a more avid binder of Sp3 than the Purβ III intermolecular subdomain (Figure 8 and Figure S10). As Sp1 and Sp3 are known to interact with several sequence elements located within the composite MCAT/CArG/GC box enhancer (20), it is quite possible that the relatively strong repressor activity of Purβ I-II observed in transfected cells was due, in part, to its ability to bind and sequester Sp3 away from the enhancer. This would also explain why Purβ I-II retained repressor activity in the face of its relatively weak ssDNA-binding affinity compared to Purβ I-II-III. On the other hand, all three PUR repeats were required for efficient interaction of Purβ with MSY1 (mouse YB-1), the co-repressor protein that interacts with the pyrimidine-rich antisense strand of the *ACTA2* Pur/Pyr tract (17, 22). This feature may account for why Purβ I-II-III was such an effective repressor when expressed in cells as direct physical interaction between Purβ and MSY1 is probably essential for efficient assembly of these co-repressors on the Pur/Pyr element and ensuing disruption of the core MCAT motif (37). Coordinated binding of MSY1 to the pyrimidine-rich strand may also serve to potentiate the intrinsic helix-destabilizing activity of Purβ (28). Unraveling the degree to which Purβ can stably alter the secondary structure of specific *cis*-elements in *ACTA2* will clearly require a more systematic evaluation of the helix-destabilizing properties of Purβ and its isolated subdomains based on the biochemical criteria established for Purα-mediated melting of duplex DNA (27, 28, 69).

In summary, our findings reveal that Purβ is a potent inhibitor of myofibroblast differentiation by virtue of its ability to repress *ACTA2* transcription via specific protein-ssDNA and protein-protein interactions. The functionally relevant unit of Purβ that mediates *ACTA2* repression appears to be the homodimeric form of the protein. Subdomain-specific inter- and intramolecular interactions account for the formation of three separate ssDNA-binding modules within the Purβ homodimer. The tripartite organization of the assembled homodimer readily explains the structural basis for the cooperative binding of Purβ to multiple purine-rich sites within the MCAT region of the composite *ACTA2* enhancer as well as the preferential association of Purβ with its co-repressor partner MSY1/YB-1.

Supplementary Material

Refer to Web version on PubMed Central for supplementary material.

References

1. Walker GA, Guerrero IA, Leinwand LA. Myofibroblasts: molecular crossdressers. Curr Top Dev Biol. 2001; 51:91–107. [PubMed: 11236717]

2. Tomasek JJ, Gabbiani G, Hinz B, Chaponnier C, Brown RA. Myofibroblasts and mechano-regulation of connective tissue remodelling. Nat Rev Mol Cell Biol. 2002; 3:349–363. [PubMed: 11988769]
3. Gabbiani G, Ryan GB, Majne G. Presence of modified fibroblasts in granulation tissue and their possible role in wound contraction. Experientia. 1971; 27:549–550. [PubMed: 5132594]
4. Gabbiani G, Hirschel BJ, Ryan GB, Statkov PR, Majno G. Granulation tissue as a contractile organ. A study of structure and function. J Exp Med. 1972; 135:719–734. [PubMed: 4336123]
5. Hinz B. Formation and function of the myofibroblast during tissue repair. J Invest Dermatol. 2007; 127:526–537. [PubMed: 17299435]
6. Hinz B, Phan SH, Thannickal VJ, Galli A, Bochaton-Piallat ML, Gabbiani G. The myofibroblast: one function, multiple origins. Am J Pathol. 2007; 170:1807–1816. [PubMed: 17525249]
7. De Wever O, Mareel M. Role of tissue stroma in cancer cell invasion. J Pathol. 2003; 200:429–447. [PubMed: 12845611]
8. Zalewski A, Shi Y, Johnson AG. Diverse origin of intimal cells: smooth muscle cells, myofibroblasts, fibroblasts, and beyond? Circ Res. 2002; 91:652–655. [PubMed: 12386139]
9. Hao H, Gabbiani G, Camenzind E, Bacchetta M, Virmani R, Bochaton-Piallat ML. Phenotypic modulation of intima and media smooth muscle cells in fatal cases of coronary artery lesion. Arterioscler Thromb Vasc Biol. 2006; 26:326–332. [PubMed: 16339500]
10. Darby I, Skalli O, Gabbiani G. Alpha-smooth muscle actin is transiently expressed by myofibroblasts during experimental wound healing. Lab Invest. 1990; 63:21–29. [PubMed: 2197503]
11. Wang J, Zohar R, McCulloch CA. Multiple roles of alpha-smooth muscle actin in mechanotransduction. Exp Cell Res. 2006; 312:205–214. [PubMed: 16325810]
12. Hinz B, Celetta G, Tomasek JJ, Gabbiani G, Chaponnier C. Alpha-smooth muscle actin expression upregulates fibroblast contractile activity. Mol Biol Cell. 2001; 12:2730–2741. [PubMed: 11553712]
13. Stoflet ES, Schmidt LJ, Elder PK, Korf GM, Foster DN, Strauch AR, Getz MJ. Activation of a muscle-specific actin gene promoter in serum-stimulated fibroblasts. Mol Biol Cell. 1992; 3:1073–1083. [PubMed: 1421567]
14. Foster DN, Min B, Foster LK, Stoflet ES, Sun S, Getz MJ, Strauch AR. Positive and negative cis-acting regulatory elements mediate expression of the mouse vascular smooth muscle alpha-actin gene. J Biol Chem. 1992; 267:11995–12003. [PubMed: 1601869]
15. Sun S, Stoflet ES, Cogan JG, Strauch AR, Getz MJ. Negative regulation of the vascular smooth muscle alpha-actin gene in fibroblasts and myoblasts: disruption of enhancer function by sequence-specific single-stranded-DNA-binding proteins. Mol Cell Biol. 1995; 15:2429–2436. [PubMed: 7739527]
16. Subramanian SV, Polikandriotis JA, Kelm RJ Jr, David JJ, Orosz CG, Strauch AR. Induction of vascular smooth muscle alpha-actin gene transcription in transforming growth factor beta1-activated myofibroblasts mediated by dynamic interplay between the Pur repressor proteins and Sp1/Smad coactivators. Mol Biol Cell. 2004; 15:4532–4543. [PubMed: 15282343]
17. Carlini LE, Getz MJ, Strauch AR, Kelm RJ Jr. Cryptic MCAT enhancer regulation in fibroblasts and smooth muscle cells. Suppression of TEF-1 mediated activation by the single-stranded DNA-binding proteins, Pur alpha, Pur beta, and MSY1. J Biol Chem. 2002; 277:8682–8692. [PubMed: 11751932]
18. Gan Q, Yoshida T, Li J, Owens GK. Smooth muscle cells and myofibroblasts use distinct transcriptional mechanisms for smooth muscle alpha-actin expression. Circ Res. 2007; 101:883–892. [PubMed: 17823374]
19. Sandbo N, Kregel S, Taurin S, Bhorade S, Dulin NO. Critical role of serum response factor in pulmonary myofibroblast differentiation induced by TGF-beta. Am J Respir Cell Mol Biol. 2009; 41:332–338. [PubMed: 19151320]
20. Cogan JG, Subramanian SV, Polikandriotis JA, Kelm RJ Jr, Strauch AR. Vascular smooth muscle alpha-actin gene transcription during myofibroblast differentiation requires Sp1/3 protein binding proximal to the MCAT enhancer. J Biol Chem. 2002; 277:36433–36442. [PubMed: 12110667]

21. Cogan JG, Sun S, Stoflet ES, Schmidt LJ, Getz MJ, Strauch AR. Plasticity of vascular smooth muscle alpha-actin gene transcription. Characterization of multiple, single-, and double-strand specific DNA-binding proteins in myoblasts and fibroblasts. J Biol Chem. 1995; 270:11310–11321. [PubMed: 7744768]
22. Kelm RJ Jr, Cogan JG, Elder PK, Strauch AR, Getz MJ. Molecular interactions between single-stranded DNA-binding proteins associated with an essential MCAT element in the mouse smooth muscle alpha-actin promoter. J Biol Chem. 1999; 274:14238–14245. [PubMed: 10318844]
23. Bergemann AD, Johnson EM. The HeLa Pur factor binds single-stranded DNA at a specific element conserved in gene flanking regions and origins of DNA replication. Mol Cell Biol. 1992; 12:1257–1265. [PubMed: 1545807]
24. Bergemann AD, Ma ZW, Johnson EM. Sequence of cDNA comprising the human pur gene and sequence-specific single-stranded-DNA-binding properties of the encoded protein. Mol Cell Biol. 1992; 12:5673–5682. [PubMed: 1448097]
25. Johnson EM, Daniel DC, Gordon J. The pur protein family: Genetic and structural features in development and disease. J Cell Physiol. 2013; 228:930–937. [PubMed: 23018800]
26. Kelm RJ Jr, Elder PK, Strauch AR, Getz MJ. Sequence of cDNAs encoding components of vascular actin single-stranded DNA-binding factor 2 establish identity to Puralpha and Purbeta. J Biol Chem. 1997; 272:26727–26733. [PubMed: 9334258]
27. Darbinian N, Gallia GL, Khalili K. Helix-destabilizing properties of the human single-stranded DNA- and RNA-binding protein Puralpha. J Cell Biochem. 2001; 80:589–595. [PubMed: 11169743]
28. Wortman MJ, Johnson EM, Bergemann AD. Mechanism of DNA binding and localized strand separation by Pur alpha and comparison with Pur family member, Pur beta. Biochim Biophys Acta. 2005; 1743:64–78. [PubMed: 15777841]
29. Kelm RJ Jr, Wang SX, Polikandriotis JA, Strauch AR. Structure/function analysis of mouse Purbeta, a single-stranded DNA-binding repressor of vascular smooth muscle alpha-actin gene transcription. J Biol Chem. 2003; 278:38749–38757. [PubMed: 12874279]
30. Knapp AM, Ramsey JE, Wang SX, Godburn KE, Strauch AR, Kelm RJ Jr. Nucleoprotein interactions governing cell type-dependent repression of the mouse smooth muscle alpha-actin promoter by single-stranded DNA-binding proteins Pur alpha and Pur beta. J Biol Chem. 2006; 281:7907–7918. [PubMed: 16436378]
31. Gupta M, Sueblinvong V, Raman J, Jeevanandam V, Gupta MP. Single-stranded DNA-binding proteins PURalpha and PURbeta bind to a purine-rich negative regulatory element of the alpha-myosin heavy chain gene and control transcriptional and translational regulation of the gene expression. Implications in the repression of alpha-myosin heavy chain during heart failure. J Biol Chem. 2003; 278:44935–44948. [PubMed: 12933792]
32. Ji J, Tsika GL, Rindt H, Schreiber KL, McCarthy JJ, Kelm RJ Jr, Tsika R. Puralpha and Purbeta collaborate with Sp3 to negatively regulate beta-myosin heavy chain gene expression during skeletal muscle inactivity. Mol Cell Biol. 2007; 27:1531–1543. [PubMed: 17145772]
33. Gupta M, Sueblinvong V, Gupta MP. The single-strand DNA/RNA-binding protein, Purbeta, regulates serum response factor (SRF)-mediated cardiac muscle gene expression. Can J Physiol Pharmacol. 2007; 85:349–359. [PubMed: 17612644]
34. McCarthy JJ, Esser KA, Peterson CA, Dupont-Versteegden EE. Evidence of MyomiR network regulation of beta-myosin heavy chain gene expression during skeletal muscle atrophy. Physiol Genomics. 2009; 39:219–226. [PubMed: 19690046]
35. van Rooij E, Quiat D, Johnson BA, Sutherland LB, Qi X, Richardson JA, Kelm RJ Jr, Olson EN. A family of microRNAs encoded by myosin genes governs myosin expression and muscle performance. Dev Cell. 2009; 17:662–673. [PubMed: 19922871]
36. Ramsey JE, Daugherty MA, Kelm RJ Jr. Hydrodynamic studies on the quaternary structure of recombinant mouse Purbeta. J Biol Chem. 2007; 282:1552–1560. [PubMed: 17121857]
37. Ramsey JE, Kelm RJ Jr. Mechanism of strand-specific smooth muscle alpha-actin enhancer interaction by purine-rich element binding protein B (Purbeta). Biochemistry. 2009; 48:6348–6360. [PubMed: 19496623]

38. Graebsch A, Roche S, Kostrewa D, Soding J, Niessing D. Of bits and bugs--on the use of bioinformatics and a bacterial crystal structure to solve a eukaryotic repeat-protein structure. PLoS One. 2010; 5:e13402. [PubMed: 20976240]
39. Graebsch A, Roche S, Niessing D. X-ray structure of Pur-alpha reveals a Whirly-like fold and an unusual nucleic-acid binding surface. Proc Natl Acad Sci U S A. 2009; 106:18521–18526. [PubMed: 19846792]
40. Rumora AE, Steere AN, Ramsey JE, Knapp AM, Ballif BA, Kelm RJ Jr. Isolation and characterization of the core single-stranded DNA-binding domain of purine-rich element binding protein B (Purbeta). Biochem Biophys Res Commun. 2010; 400:340–345. [PubMed: 20728429]
41. Wang J, Niu W, Nikiforov Y, Naito S, Chernausek S, Witte D, LeRoith D, Strauch A, Fagin JA. Targeted overexpression of IGF-I evokes distinct patterns of organ remodeling in smooth muscle cell tissue beds of transgenic mice. J Clin Invest. 1997; 100:1425–1439. [PubMed: 9294108]
42. Larkin MA, Blackshields G, Brown NP, Chenna R, McGettigan PA, McWilliam H, Valentin F, Wallace IM, Wilm A, Lopez R, Thompson JD, Gibson TJ, Higgins DG. Clustal W and Clustal X version 2.0. Bioinformatics. 2007; 23:2947–2948. [PubMed: 17846036]
43. Goujon M, McWilliam H, Li W, Valentin F, Squizzato S, Paern J, Lopez R. A new bioinformatics analysis tools framework at EMBL-EBI. Nucleic Acids Res. 2010; 38:W695–699. [PubMed: 20439314]
44. Biegert A, Soding J. De novo identification of highly diverged protein repeats by probabilistic consistency. Bioinformatics. 2008; 24:807–814. [PubMed: 18245125]
45. Buchan DW, Ward SM, Lobley AE, Nugent TC, Bryson K, Jones DT. Protein annotation and modelling servers at University College London. Nucleic Acids Res. 2010; 38:W563–568. [PubMed: 20507913]
46. Zhang Y. I-TASSER server for protein 3D structure prediction. BMC Bioinformatics. 2008; 9:40. [PubMed: 18215316]
47. Roy A, Kucukural A, Zhang Y. I-TASSER: a unified platform for automated protein structure and function prediction. Nat Protoc. 2010; 5:725–738. [PubMed: 20360767]
48. Arnold K, Bordoli L, Kopp J, Schwede T. The SWISS-MODEL workspace: a web-based environment for protein structure homology modelling. Bioinformatics. 2006; 22:195–201. [PubMed: 16301204]
49. Kiefer F, Arnold K, Kunzli M, Bordoli L, Schwede T. The SWISS-MODEL Repository and associated resources. Nucleic Acids Res. 2009; 37:D387–392. [PubMed: 18931379]
50. Bordoli L, Kiefer F, Arnold K, Benkert P, Battey J, Schwede T. Protein structure homology modeling using SWISS-MODEL workspace. Nat Protoc. 2009; 4:1–13. [PubMed: 19131951]
51. Emsley P, Lohkamp B, Scott WG, Cowtan K. Features and development of Coot. Acta Crystallogr D Biol Crystallogr. 2010; 66:486–501. [PubMed: 20383002]
52. Brunger AT, Adams PD, Clore GM, DeLano WL, Gros P, Grosse-Kunstleve RW, Jiang JS, Kuszewski J, Nilges M, Pannu NS, Read RJ, Rice LM, Simonson T, Warren GL. Crystallography & NMR system: A new software suite for macromolecular structure determination. Acta Crystallogr D Biol Crystallogr. 1998; 54:905–921. [PubMed: 9757107]
53. Brunger AT. Version 1.2 of the Crystallography and NMR system. Nat Protoc. 2007; 2:2728–2733. [PubMed: 18007608]
54. Schrodinger LLC. The PyMOL Molecular Graphics System. Version 1.3r1. 2010
55. Gasteiger E, Gattiker A, Hoogland C, Ivanyi I, Appel RD, Bairoch A. ExPASy: The proteomics server for in-depth protein knowledge and analysis. Nucleic Acids Res. 2003; 31:3784–3788. [PubMed: 12824418]
56. Knapp AM, Ramsey JE, Wang SX, Strauch AR, Kelm RJ Jr. Structure-function analysis of mouse Pur beta II. Conformation altering mutations disrupt single-stranded DNA and protein interactions crucial to smooth muscle alpha-actin gene repression. J Biol Chem. 2007; 282:35899–35909. [PubMed: 17906292]
57. Wang SX, Elder PK, Zheng Y, Strauch AR, Kelm RJ Jr. Cell cycle-mediated regulation of smooth muscle alpha-actin gene transcription in fibroblasts and vascular smooth muscle cells involves multiple adenovirus E1A-interacting cofactors. J Biol Chem. 2005; 280:6204–6214. [PubMed: 15576380]

58. Becker NA, Kelm RJ Jr, Vrana JA, Getz MJ, Maher LJ 3rd. Altered sensitivity to single-strand-specific reagents associated with the genomic vascular smooth muscle alpha-actin promoter during myofibroblast differentiation. J Biol Chem. 2000; 275:15384–15391. [PubMed: 10748152]
59. White MK, Johnson EM, Khalili K. Multiple roles for Puralpha in cellular and viral regulation. Cell Cycle. 2009; 8:1–7. [PubMed: 19182532]
60. Ronnov-Jessen L, Petersen OW. A function for filamentous alpha-smooth muscle actin: retardation of motility in fibroblasts. J Cell Biol. 1996; 134:67–80. [PubMed: 8698823]
61. Hinz B, Phan SH, Thannickal VJ, Prunotto M, Desmouliere A, Varga J, De Wever O, Mareel M, Gabbiani G. Recent developments in myofibroblast biology: paradigms for connective tissue remodeling. Am J Pathol. 2012; 180:1340–1355. [PubMed: 22387320]
62. Zhang A, David JJ, Subramanian SV, Liu X, Fuerst MD, Zhao X, Leier CV, Orosz CG, Kelm RJ Jr, Strauch AR. Serum response factor neutralizes Pur alpha- and Pur beta-mediated repression of the fetal vascular smooth muscle alpha-actin gene in stressed adult cardiomyocytes. Am J Physiol Cell Physiol. 2008; 294:C702–714. [PubMed: 18344281]
63. Johnson EM, Chen PL, Krachmarov CP, Barr SM, Kanovsky M, Ma ZW, Lee WH. Association of human Pur alpha with the retinoblastoma protein, Rb, regulates binding to the single-stranded DNA Pur alpha recognition element. J Biol Chem. 1995; 270:24352–24360. [PubMed: 7592647]
64. Barr SM, Johnson EM. Ras-induced colony formation and anchorage-independent growth inhibited by elevated expression of Puralpha in NIH3T3 cells. J Cell Biochem. 2001; 81:621–638. [PubMed: 11329617]
65. Khalili K, Del Valle L, Muralidharan V, Gault WJ, Darbinian N, Otte J, Meier E, Johnson EM, Daniel DC, Kinoshita Y, Amini S, Gordon J. Puralpha is essential for postnatal brain development and developmentally coupled cellular proliferation as revealed by genetic inactivation in the mouse. Mol Cell Biol. 2003; 23:6857–6875. [PubMed: 12972605]
66. Liu H, Barr SM, Chu C, Kohtz DS, Kinoshita Y, Johnson EM. Functional interaction of Puralpha with the Cdk2 moiety of cyclin A/Cdk2. Biochem Biophys Res Commun. 2005; 328:851–857. [PubMed: 15707957]
67. Darbinian N, Gallia GL, Kundu M, Shcherbik N, Tretiakova A, Giordano A, Khalili K. Association of Pur alpha and E2F-1 suppresses transcriptional activity of E2F-1. Oncogene. 1999; 18:6398–6402. [PubMed: 10597240]
68. Darbinian N, White MK, Gallia GL, Amini S, Rappaport J, Khalili K. Interaction between the pura and E2F-1 transcription factors. Anticancer Res. 2004; 24:2585–2594. [PubMed: 15517862]
69. Zhang Q, Pedigo N, Shenoy S, Khalili K, Kaetzel DM. Puralpha activates PDGF-A gene transcription via interactions with a G-rich, single-stranded region of the promoter. Gene. 2005; 348:25–32. [PubMed: 15777709]

Abbreviations

SMαA	smooth muscle α-actin
ssDNA	single-stranded DNA
MEF	mouse embryo fibroblast
MCAT	muscle CAT
Pur/Pyr	polypurine/polypyrimidine
YB-1	Y-box binding protein 1
AoSMC	aortic outgrowth smooth muscle cell
TGF-β1	transforming growth factor β1

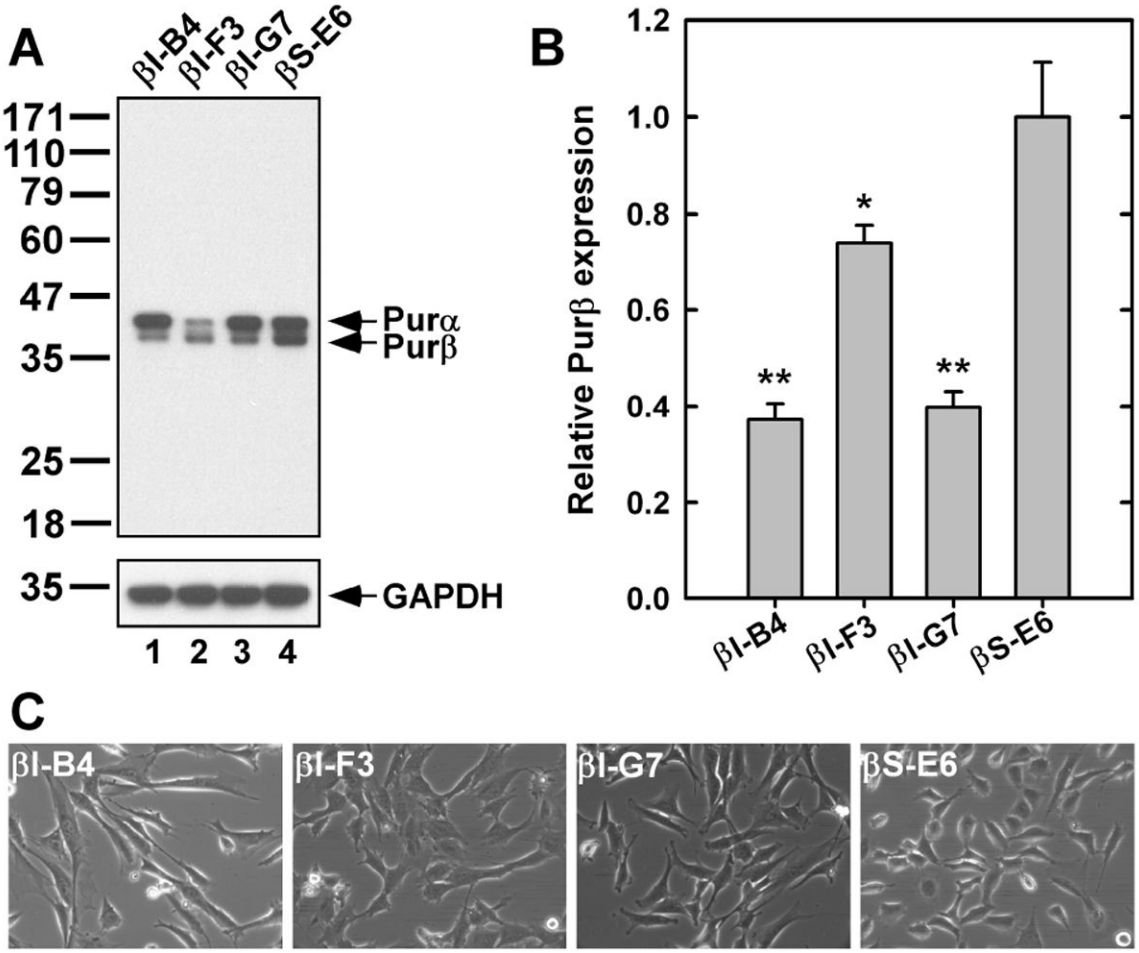

Figure 1.

Validation of constitutive Purβ knockdown in MEFs. (A) Immunoblotting of whole cell extracts (10 μg protein/lane) from the indicated MEF cell lines was conducted with a mAb (rat anti-Purβ 42-69 clone 3C3.6C1) directed against a conserved PUR repeat I epitope present in both Purα (slower migrating band) and Purβ (faster migrating band). The Purα/β blot was reprobed with a GAPDH mAb to confirm equivalent protein loading. βI-B4 and βI-G7 (lanes 1 and 3) are two distinct clonal cell lines stably expressing a Purβ shRNA, while βS-E6 is a control cell line stably expressing a scrambled RNA (lane 4). For the purpose of comparison, βI-F3 (lane 2) is a serendipitously isolated cell line deficient in Purα expression. Lines and numbers on the left side designate the relative position and size (in kDa) of prestained protein markers. (B) Quantification of functional Purβ protein in extracts from the indicated MEF cell lines by ssDNA-binding ELISA. Bars show Purβ expression relative to βS-E6 control cells (mean ± SEM, n = 4). *, $p < 0.05$, **, $p < 0.01$ compared to βS-E6. (C) Phase contrast micrographs of subconfluent cultures of the indicated MEF cell lines viewed through a 20× objective.

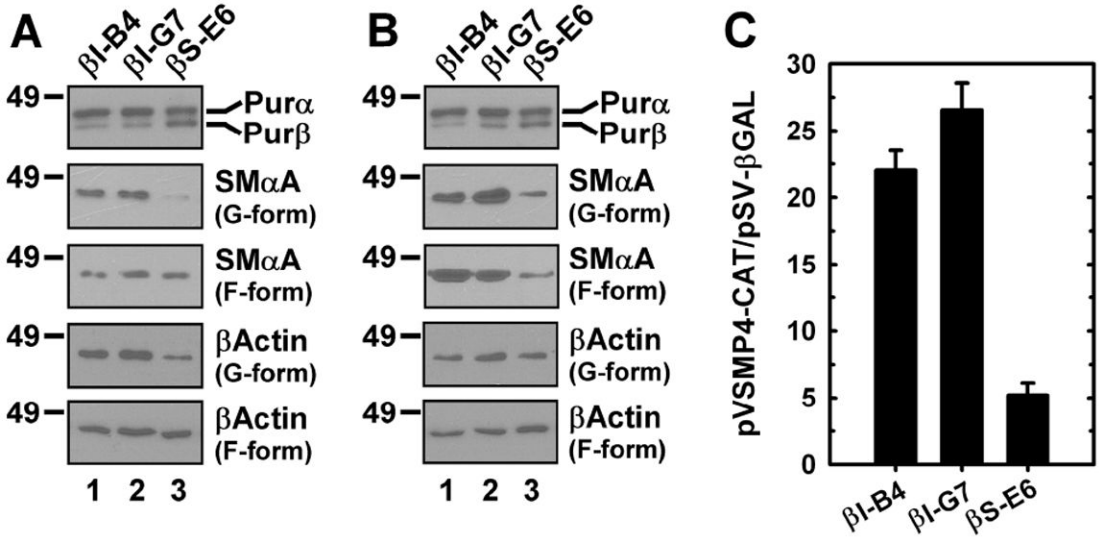

Figure 2.

Knockdown of Purβ enhances SMαA expression in growth factor-stimulated MEFs. (A, B) Immunoblotting of cell extracts prepared from Purβ knockdown (lanes 1 and 2) and control (lane 3) MEFs stimulated with either serum (A) or TGF-β1 (B) was conducted with mAbs against Purα/β, SMαA, or β-actin. Purα/β (10 μg protein/lane) and G-form actin (0.5 μg protein/lane) were detected in detergent-soluble cell lysates. F-form actins were detected in detergent-insoluble cell remnants dissolved in 8 M urea (0.2 μg protein loaded/lane). (C) The indicated MEF cell lines were transiently transfected with a combination of pVSMP4-CAT and pSV-βgal promoter-reporter constructs. Cell extracts were prepared 48 h later and reporter enzymes were quantified by ELISA. Bars show the ratio of CAT to β-gal measured in each cell line normalized for total protein (mean ± SEM).

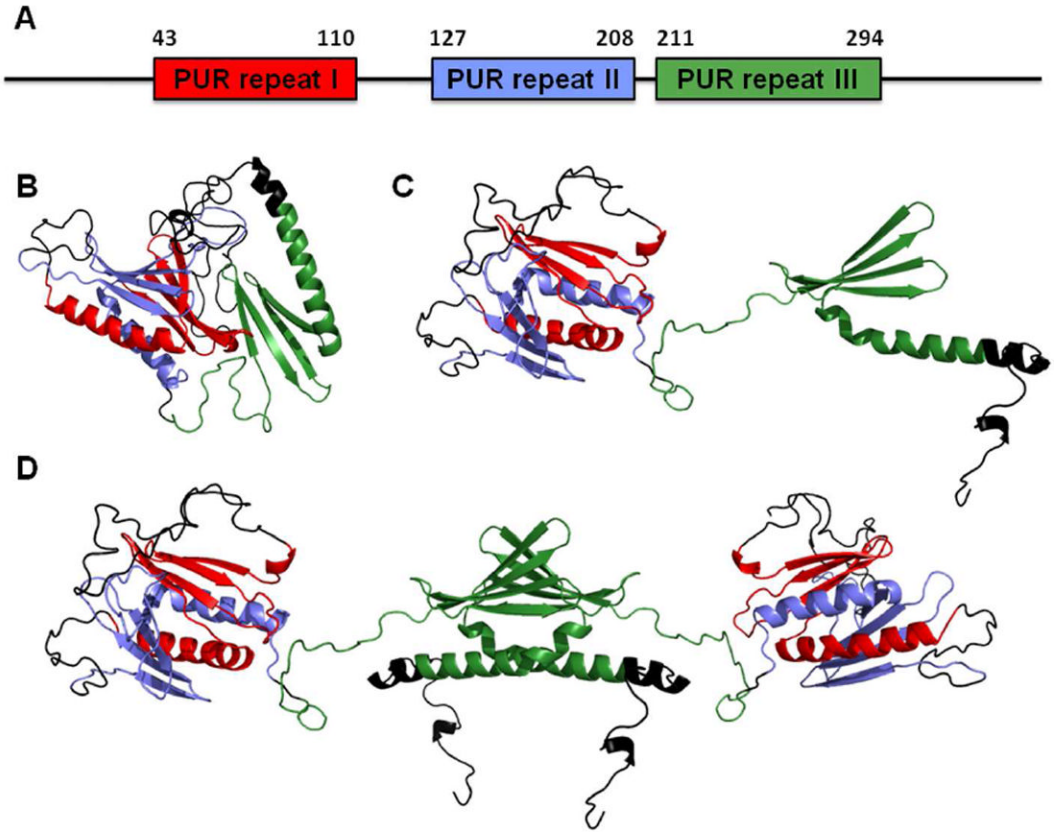

Figure 3.

Computational models of *Mm* Purβ monomer and dimer. (A) The primary sequence of the 324 amino acid *Mm* Purβ was analyzed by HHrepID. Predicted regions corresponding to PUR repeats I, II, and III are highlighted in red, blue, and green, respectively. Numbers refer to amino acid positions. Intervening elements and N-and C-terminal regions are shown as black lines. (B) Web servers (I-TASSER and SWISS-MODEL) were used to generate a homology model of the Purβ monomer. In this hypothetical model, PUR repeat III (green) is in a closed conformation relative to the intramolecular PUR domain formed by PUR repeats I (red) and II (blue). (C) A model of the Purβ monomer in an extended conformation was generated by rotating the PUR repeat III away from the intramolecular domain formed by PUR repeats I-II. (D) A model of the Purβ dimer was created by aligning the PUR III repeats of two Purβ monomers in such a way as to form an intermolecular PUR domain that is predicted to mediate protein self-association.

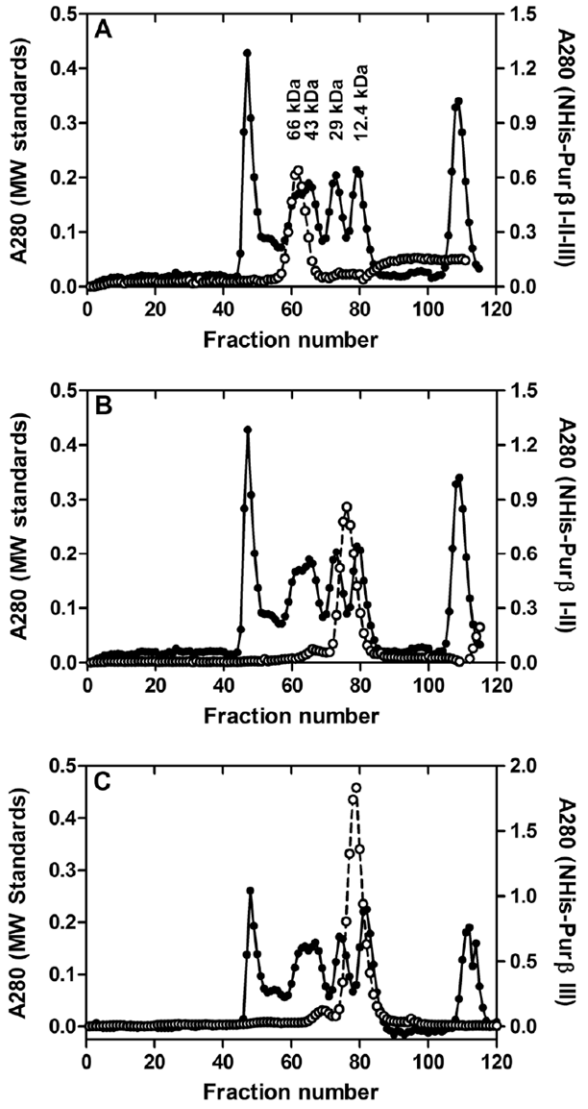

Figure 4.

Quaternary structure of isolated Purβ subdomains. (A-C) Calibrated SEC was conducted on preparations of Purβ I-II-III (A), Purβ I-II (B), and Purβ III (C) at loading concentrations in excess of 10 μM (open circles). The elution profile of a mixture of molecular weight standards is shown for comparison (closed circles). Numbers in (A) indicate the apparent molecular weights of the four globular protein standards used in generating a standard curve to calculate the size of the Purβ species eluting in the peak fractions.

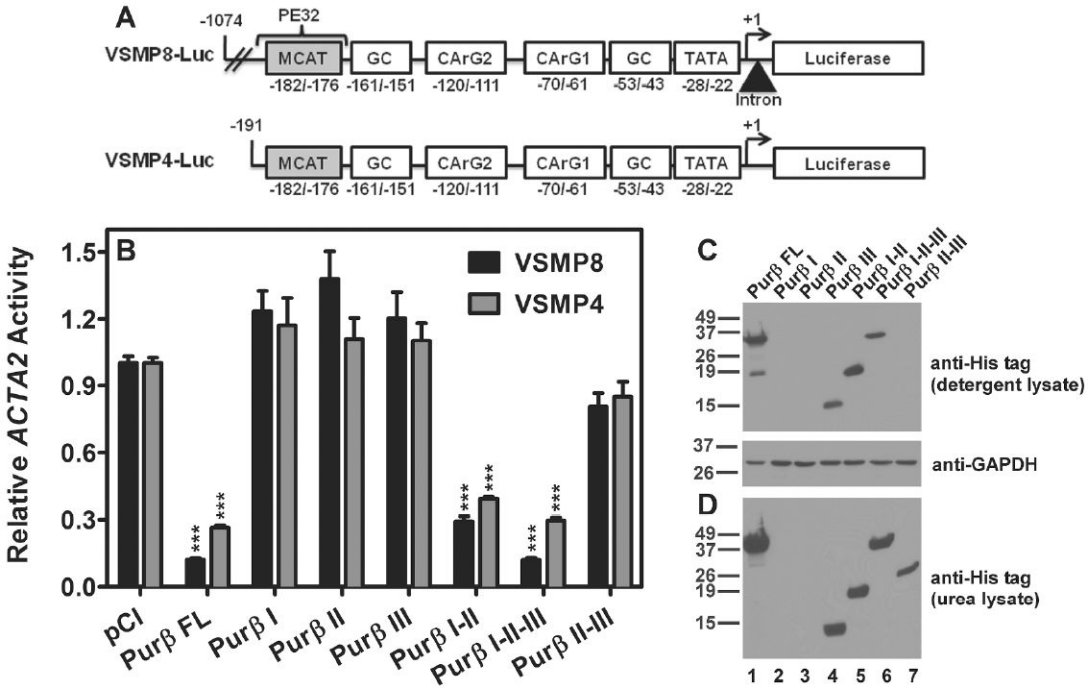

Figure 5.

ACTA2 repressor activity of Purβ truncation proteins expressed in AKR-2B MEFs. (A) Schematic representation of the full-length (VSMP8-Luc) and truncated (VSMP4-Luc) *ACTA2* promoter-reporter constructs used to assess Purβ repressor function. PE32 designates the Purβ recognition sequence containing an MCAT motif. (B) Subconfluent AKR-2B MEFs were transiently co-transfected with *ACTA2* luciferase reporters and expression vectors encoding the indicated Purβ proteins. After 48 h, cell lysates were prepared and assayed for luciferase activity and total protein. Bars show total protein-corrected luciferase values normalized to the pCI control (defined as 1) for each reporter (mean ± SEM, n = 9). ***, $p < 0.001$ compared to pCI control for VSMP8 (black bars) or VSMP4 (gray bars). (C) Western blotting of detergent-soluble lysates (15 μg protein/lane) of transfected cells was performed with a mAb recognizing the N-terminal His epitope tag present on each Purβ construct. The anti-His tag blot was reprobed with a GAPDH mAb as a loading control. (D) Western blotting of urea-denatured lysates (15 μg protein/lane) of detergent-insoluble cell remnants was conducted with the His tag mAb. (C, D) In both immunoblots, lysates were resolved on a 15% polyacrylamide gel. Lines and numbers on the left side designate the relative position and size (in kDa) of prestained protein markers. FL, full-length.

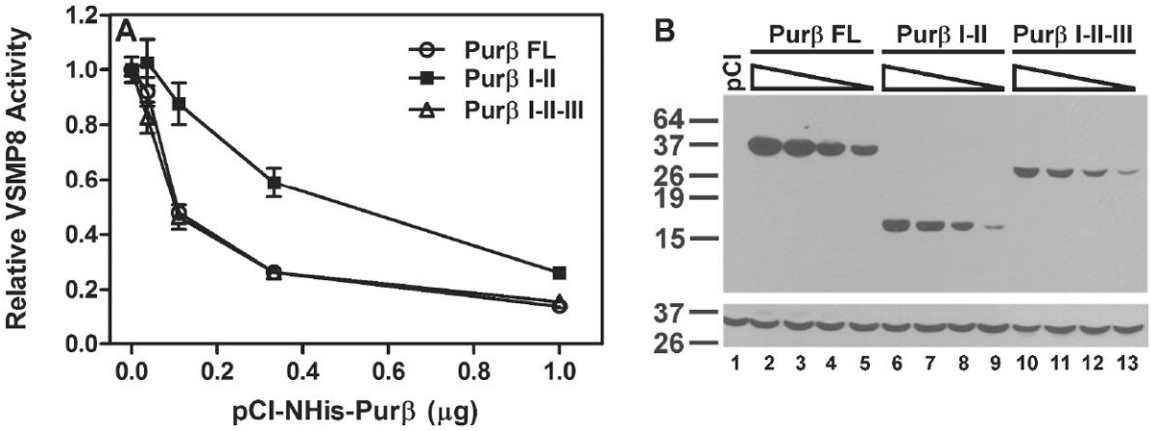

Figure 6.

Relative *ACTA2* repressor activity of Purβ truncation proteins expressed in AKR-2B MEFs. (A) AKR-2B MEFs were transiently co-transfected with a fixed amount of *ACTA2* luciferase reporter (VSMP8) and varying amounts of expression vector encoding the indicated Purβ proteins. After 48 h, cell lysates were prepared and assayed for luciferase activity and total protein. Symbols show total protein-corrected luciferase values normalized to the pCI control (mean ± SEM, n = 6). (B) Immunoblots of transfected cell lysates (15 μg protein/lane) with a His tag mAb (top panel) followed by a GAPDH mAb (lower panel). Lines and numbers on the left side designate the relative position and size (in kDa) of prestained protein markers. FL, full-length.

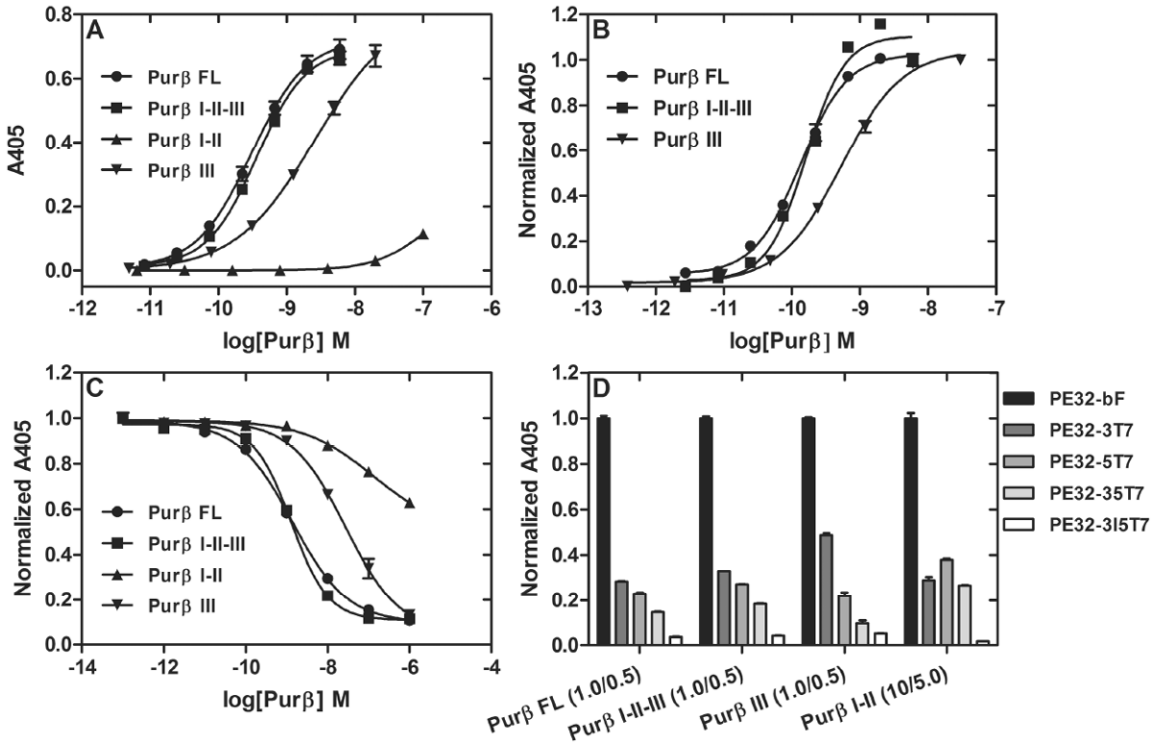

Figure 7.

The relative affinity and specificity of Purβ truncation proteins for ssDNA. (A, B) Varying concentrations of the indicated NHis-Purβ proteins were incubated with 0.5 nM biotinylated mouse *ACTA2*-derived ssDNA probe (PE32-bF) immobilized on StreptaWells. (A) Solid-phase nucleoprotein complexes were detected by ELISA using a primary antibody recognizing the NHis tag. Absorbance values at 405 nm (A405) were corrected for nonspecific binding by subtracting the signal generated in wells with no DNA. (B) Solid-phase nucleoprotein complexes were detected by ELISA using a primary antibody directed against amino acids 210-229 of Purβ. A405 values were corrected for nonspecific binding and normalized to the absorbance obtained at the maximum concentration of each protein tested (defined as 1). (C) Varying concentrations of fluid-phase Purβ proteins were incubated with a fixed concentration of PE32-bF (0.5 nM) in microtiter wells pre-coated with full-length Purβ (20 nM). Solid-phase nucleoprotein complexes were detected by colorimetric assay using an avidin-peroxidase conjugate. A405 values were normalized to the maximum absorbance obtained in the absence of any competitor. (A, B, and C) Data points were fit to a four parameter equation to determine an EC50 (A, B) or IC50 (C) for each protein. A representative experiment is shown in each panel. (D) A fixed concentration of Purβ protein was incubated with wild type or mutant ssDNA probes immobilized on StreptaWells. The ratio of Purβ to ssDNA tested (nM/nM) is indicated in parentheses. Solid-phase nucleoprotein complexes were detected by ELISA with a primary His tag antibody. A405 values were corrected for nonspecific binding and normalized to the absorbance obtained for each protein binding to the wild type probe (defined as 1). FL, full-length.

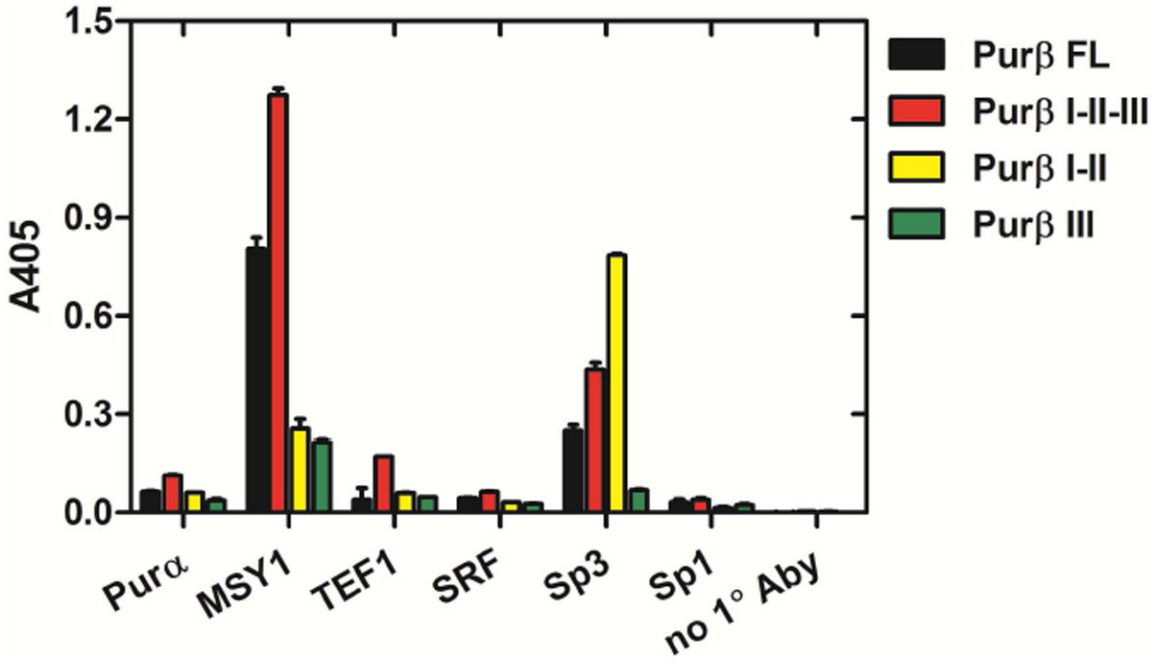

Figure 8.

Relative binding of AKR-2B MEF-derived transcription factors to purified NHis-Purβ proteins. Microtiter wells coated with equivalent concentrations of the indicated Purβ proteins (200 nM) were incubated with a fixed amount of nuclear protein (250 μg/ml) diluted in binding buffer. Solid-phase protein-protein complexes were detected by ELISA using primary rabbit polyclonal antibodies recognizing Purα, MSY1, TEF1, SRF, Sp3, or Sp1. Absorbance values at 405 nm generated with each transcription factor antibody were corrected for nonspecific antibody binding to Purβ coated wells in the absence of nuclear extract. Signal generated in Purβ-coated wells incubated with nuclear extract and probed with the secondary antibody only (no 1° Aby) is shown as a background control. FL, full-length.